ACS OMEGA

http://pubs.acs.org/journal/acsodf

Article

Radix Pueraria Flavonoids Assisted Green Synthesis of Reduced Gold Nanoparticles: Application for Electrochemical Nonenzymatic Detection of Cholesterol in Food Samples

Bolin Han, Huanan Guan,* Yan Song, and Ying Liu*

Cite This: *ACS Omega* 2022, 7, 43045−43054

Read Online

ACCESS | Metrics & More | Article Recommendations

ABSTRACT: Using radix pueraria flavonoids (RPFs) as a reducing and stabilizing agent, we report a simple, cost-effective, and ecologically friendly green synthesis technique for gold nanoparticles (AuNPs) in the present study. Ultraviolet−visible (UV) spectroscopy, transmission electron microscopy (TEM), Fourier transform infrared (FTIR), and X-ray diffraction (XRD) investigations were used to characterize the AuNPs. The results demonstrated that the produced AuNPs were nearly spherical and that their particle sizes had a mean diameter of 4.85 ± 0.75 nm. The "Green" AuNPs, exhibiting remarkable peroxidase-like activity and Michaelis−Menten kinetics with high affinity for H_2O_2 and 3,3′,5,5′-tetramethylbenzidine (TMB), were effectively applied to the fabrication of a sensitive nonenzymatic enhanced electrochemical sensor for the detection of cholesterol (Cho). Under optimum circumstances, it was possible to establish two linear ranges of 1−100 and 250−5000 μmol/L with a detection limit of 0.259 μmol/L (signal/noise ratio (S/N) = 3). The suggested sensor was utilized with satisfactory findings to determine the amount of Cho in food samples.

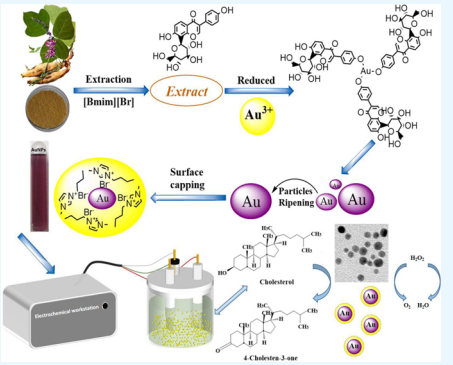

1. INTRODUCTION

Gold nanoparticles (AuNPs), the most stable metal nanoparticles, have distinctive physicochemical properties such as a large surface-to-volume ratio, catalytic properties, magnetic properties, chemical properties, distinct optoelectronic characteristics, and excellent biocompatibility and a wide range of applications. These applications include chemical catalysis,[1] electronic and magnetic devices,[2] biomedicine,[3] biosensing,[4] and nanotechnology.[5] Typically, AuNPs are generated utilizing colloidal chemistry techniques involving sodium borohydride and sodium citrate.[6] Nevertheless, despite their numerous benefits, the chemical reducing agents used in specific synthesis techniques are harmful or poisonous.

The green synthesis of nanoparticles has been the subject of research because of its advantages, which include being environmentally friendly, cost-effective, and simple to prepare. One of the most effective methods is producing metallic nanoparticles utilizing plants, algae, fungi, bacteria, and viruses.[7] In contrast, plant-mediated biological nanoparticle synthesis has more significant benefits than microbial synthesis since it overcomes the major disadvantage of being unable to provide superior control over nanoparticle size distribution, shape, and crystallinity.[8] Due to the availability of numerous phytochemicals, different plant extracts such as plant, flower, root, fruit, and leaf are extensively utilized to synthesize various nanoparticles (i.e., ascorbic and citric acids, tannins, flavonoids, terpenoids, quinones, phenolic acids, and proteins).[9,10] Particularly, plant-mediated nanoparticles incorporate the biocompatibility of phytochemicals, hence expanding their usefulness. Flavonoids, which are prevalent in plants such as vegetables, fruits, and traditional Chinese herbal medicine, are reported to be the active biological molecules responsible for lowering AuNPs.[11]

Radix puerariae (RP) is rich in flavonoids and other bioactive chemicals, such as puerarin, daidzin, and daidzein, and has been utilized in China for a range of illness prevention and treatment reasons as herbal medicine and functional food raw material.[12−14] Hydroxyl and carbonyl groups are the primary constituents of the RP extract. Both functional groups enable plant extract to behave as a reducing and stabilizing agent. The extracted flavonoids functionalize the generated AuNPs. Ionic liquids (ILs) can be used as excellent stabilizing ligands for the synthesis of stable metal nanoparticles because they have been shown to control the agglomeration of AuNPs in conventional chemical synthesis.[11] Moreover, they possess superior extraction efficiency for flavonoids and other biological functional groups.[15]

Received: August 20, 2022
Accepted: November 4, 2022
Published: November 16, 2022

https://doi.org/10.1021/acsomega.2c05358
ACS Omega 2022, 7, 43045−43054

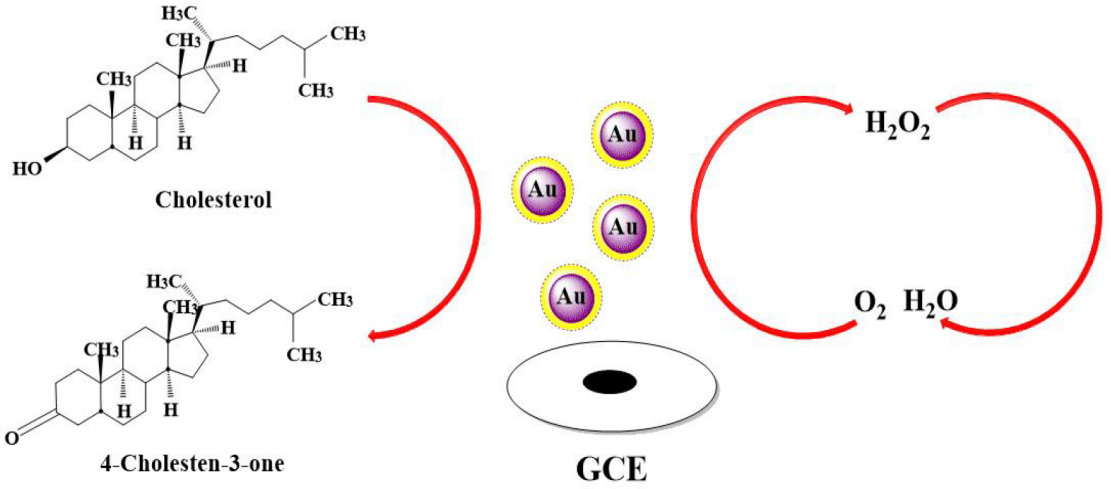

Figure 1. Schematic presentation of the electrochemical sensor based on peroxidase-like activity of RPF-AuNPs for the detection of Cho.

Cholesterol (Cho) is an organic molecule that plays an important role in human health. Its overproduction or underproduction can result in health problems. Food and liver biosynthesis are the primary sources of Cho.[16] As a result, detecting the Cho sensitively and accurately is critical for disease control and prevention. Several methods for determining Cho have been published, including high performance liquid chromatography (HPLC),[17] colorimetry,[18] fluorimetry,[19] and electrochemistry methods.[20−23] Among them, the electrochemical method is the most popular due to its rapidity, simplicity, low cost, satisfactory reproducibility, and user-friendliness.[24−27]

Due to their health benefits and eco-friendliness, radix pueraria flavonoids (RPFs) are being evaluated for use in the synthesis of biocompatible AuNPs. In addition, the determination of Cho in food is a necessary analytical activity as hypercholesterolemia has become a consequence of modern dietary practices.[28] To determine the effectiveness of a nonenzymatic improved electrochemical sensor based on the peroxidase-like activity of AuNPs for the detection of Cho, the present work described a simple technique for the biosynthesis of AuNPs utilizing IL[Bmim]Br and RPF. The principle schematic of Cho detection is illustrated in Figure 1. RPF-AuNPs show excellent electrocatalytic capabilities and create significant electrochemical oxidation peaks during the conversion of Cho to cholest-4-en-3-one and H_2O_2. Simultaneously, H_2O_2 might oxidize to create the oxidative activity radicals (·OH) catalyzed by Au^0 to further catalyze the redox reaction of Cho on the electrode surface and increase the current responsiveness. The suggested sensor provides a dependable and uncomplicated method for Cho sensing in food samples without modifying the electrode, setting a benchmark for using nanomaterial-based nonenzymatic sensors in food analysis.

2. EXPERIMENTAL SECTION

2.1. Chemicals, Reagents, and Instrumentation. Pueraria extract (P.E.) was obtained from Chenguang Biotechnology Group Co., Ltd., (Handan, China). [Bmim][Br] (≥99%) was obtained from Shanghai Aichun Biotechnology Co., Ltd. (Shanghai, China). Chloroauric acid ($HAuCl_4$), 3,3′,5,5′-tetramethylbenzidine (TMB), hydrogen peroxide (H_2O_2, 30%) and phosphate buffer saline (PBS) were purchased from Aladdin Ltd. (Shanghai, China). Cholesterol was purchased from Sigma-Aldrich (Shanghai, China). The concentration of PBS was 10.0 mmol/L. All reagents and chemicals were analytical grade and used as received without further purification. Food samples were prepared from the local supermarket (Harbin, China).

For AuNP synthesis and peroxidase activity, an ultraviolet−visible (UV) spectrophotometer (UV-2250, Beijing Shinetek Instruments Co., Ltd., China) was used. The surface topography of the synthesized AuNPs was analyzed by a transmission electron microscopy (TEM) instrument (JEM-2100, JEOL, Japan). The particle size distribution and the ξ-potential value of the synthesized AuNPs were measured using BROOKH EVEN Zeta PALS. To confirm the involvement of the desired functional groups in AuNP synthesis, the spectra were recorded in a range of 400−4000 cm^{-1} on a Fourier transform infrared (FT-IR) spectrometer (Magna-IR 560, Nicolet, USA). The crystalline phase of the AuNPs was analyzed by using X-ray diffraction (XRD) patterns (XPERTTVPVR-7130, ULVCA-PHI, USA). Electrochemical experiments were performed on the electrochemical workstation (CHI 660E, Shanghai Chenhua Instrument, China). A conventional three-electrode system consisting of an Ag/AgCl electrode as the reference electrode, a bare glassy carbon electrode (GCE, 3.0 mm in diameter) as the working electrode, and a platinum wire as the auxiliary electrode was used.

2.2. Preparation of Radix Pueraria Flavonoids. Ultrasonic treatment for 30 min at 70 °C with 250 W of ultrasonic power was applied to 0.5 g of correctly weighed radix pueraria powder. After centrifugation at 4000 rpm for 10 min, the resultant extraction was free of unwanted contaminants. The RPF supernatant was kept at 4 °C in a vial for future use. 0.5 mg/mL of the extract was produced using a stock solution of 3.7 mg/mL of the extract. Due to a decrease in reduction power with time, the flavonoid was reacted with chloroauric acid as soon as possible after production to counteract this effect.

2.3. Synthesis of RPF-AuNPs. Stirring for 10 min at 25 °C with the $HAuCl_4$ solution (0.02%, w/v) and RPF extract (0.5 mg/mL) resulted in the desired reaction. The usual reaction was carried out by adding 1 mL of the RPF extract (0.5 mg/mL). This process was halted at 4 °C when the

https://doi.org/10.1021/acsomega.2c05358
ACS Omega 2022, 7, 43045−43054

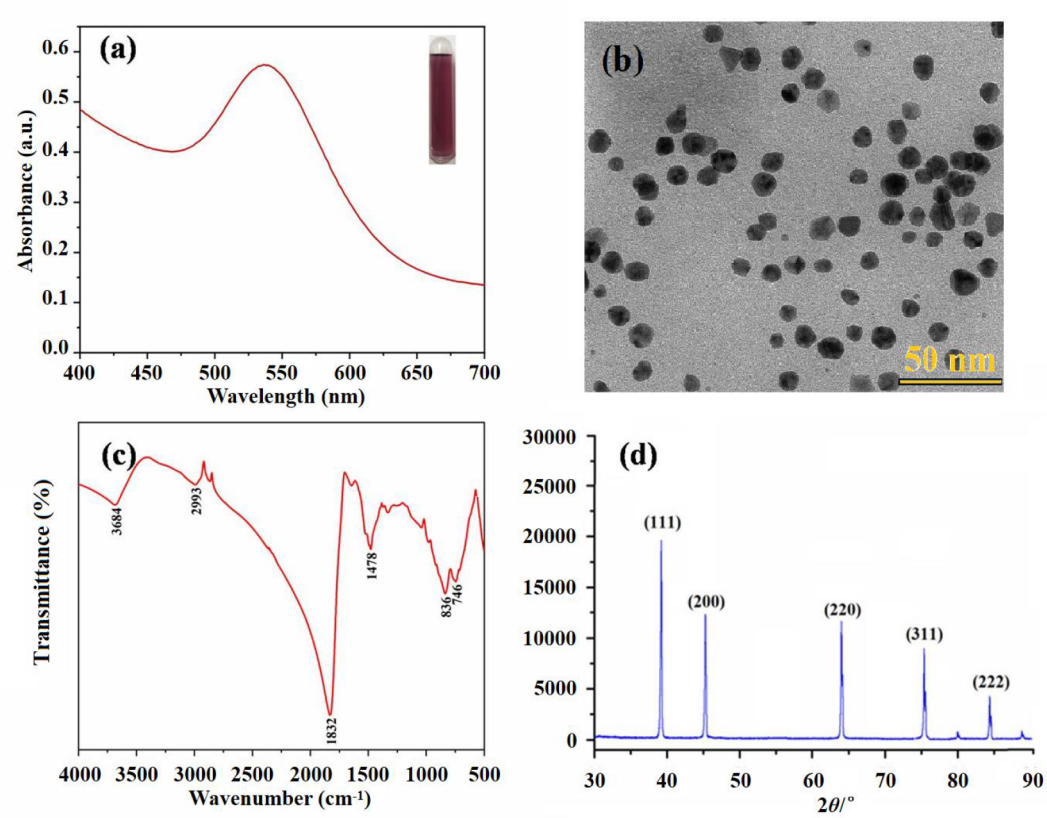

Figure 2. (a) UV−visible spectra, (b) TEM image, (c) FTIR spectra, and (d) XRD analysis of RPF-AuNPs.

solution turned wine red, indicating the production of RPF-AuNPs. The RPF-AuNP colloidal solutions were kept at 4 °C.

2.4. Peroxidase-Like Activity and the Steady-State Kinetic Assay of RPF-AuNPs. In order to investigate the peroxidase-like activity of the RPF-AuNPs that we synthesized, we used TMB as the chromogenic substrate for the oxidation reaction.

The AuNPs catalyzed TMB as a peroxidase in the presence of H_2O_2 in a previous experiment.[29] This was followed by the creation of the blue oxidation product TMB (oxTMB), which could be detected by a UV−vis spectrophotometer.

Similarly, the steady-state kinetic analysis was studied by observing the reaction system. First, the kinetic characteristics of one substrate were manipulated by altering its concentration while maintaining the concentration of another substrate. Second, a UV−vis timecourse measurement was used to record the particular absorption spectrum. Each sample was assayed three times (n = 3).

2.5. Electrochemical Nonenzymatic Detection of Cholesterol by RPF-AuNPs. The Cho nonenzymatic electrochemical detection system was carried out as follows under optimal conditions: in 9 mL of optimum pH PBS (10 mmol/L), 200 μL of RPF-AuNPs, 300 μL of cholesterol standard solution (5 mmol/L), and 500 μL of TMB (1 mmol/L). The mixture was well mixed at the ideal temperature. Various nonenzymatic electrochemical detection systems were subsequently scanned using cyclic voltammetry (CV) under ideal scan rate circumstances, and the absolute value of the oxidation peak current ($|I_{pa}|$) was measured. Each sample was assayed three times (n = 3).

2.6. Real Sample Analysis. 0.20 g of egg yolk was dissolved in 5 mL of KOH/ethanol solution and saponified at 80 °C for 20 min. After adding 10 mL of n-hexane, the mixture was agitated for 1 min and allowed to stand for 5 min. At 65 °C, a 1.0 mL aliquot of the supernatant was nearly evaporated to dryness. The extract was diluted in 4 mL of glacial acetic acid for subsequent electrochemical investigation. The 0.50 g of finely ground pork liver was dissolved in 4.5 mL of NaOH/ethanol solution and saponified in a 65 °C water bath for 1 h. After 3 mL of a 15% NaCl solution and 10 mL of n-hexane were added, the mixture was violently agitated for 2 min. After 5 min, a 2.0 mL aliquot of the supernatant was almost completely evaporated at 65 °C. For further electrochemical investigation, this sample was diluted in 4.0 mL of glacial acetic acid. The results were compared with those obtained by the HPLC method.[23]

3. RESULTS AND DISCUSSION

3.1. Characterization of RPF-AuNPs. The UV spectra of the surface plasmon resonance (SPR) band for synthesized nanoparticles is portrayed in Figure 2a. The maximum absorption wavelength was 536 nm, and the peak shape was uniform and sharp. It could be observed from the illustration that the synthesized AuNPs were wine-red. It implies a large amount of Au^{3+} ions got reduced to Au^0 when capped by the RPF extract.

Representative TEM images of gold colloids revealed that the particles were spherical and well dispersed, the RPF-AuNPs had a mean diameter of 4.85 ± 0.75 nm, and 78% (by volume) of the particles were below 10 nm with a major proportion of the suspension distributed within the window of 0.5−13.4 nm (Figure 2b). The RPF-AuNPs had a ξ-potential of −7.5 mV.

The Fourier transform infrared (FTIR) spectra of RPF-AuNPs are depicted in Figure 2c. C−H aromatic bending was

https://doi.org/10.1021/acsomega.2c05358
ACS Omega 2022, 7, 43045−43054

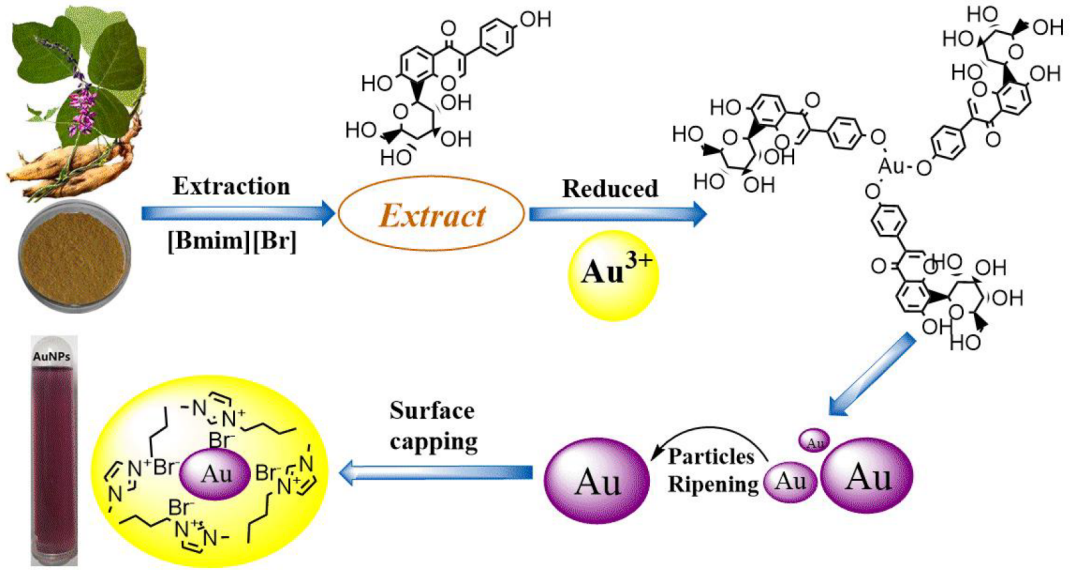

Figure 3. Possible mechanism involved in IL-mediated biosynthesis of AuNPs.

detected by the IR bands at 746 and 836 cm^{-1}. The peaks at 1478 and 2993 cm^{-1}, respectively, represent C═C aromatic vibration and C−H stretching vibration. Band at 1832 cm^{-1} were linked to the C═O stretch in anhydride. Significant band at 3684 cm^{-1} due to the O−H stretch showed terpene, phenolic, and flavonoid chemicals.[30] The presence of C═O and C═C functional groups also indicated the existence of phenol and flavonols. These functional groups suggested that phenolic and flavonoid chemicals operate as reducing agents in the production of AuNPs.[31] The band at 2993 cm^{-1} could result from the functional groups of [Bmim][Br]. The IR spectrum revealed that bioactive chemicals present in RPF were bound to the surfaces of AuNPs, and it was hypothesized that leftover plant extract components capped the nanoparticles as stabilizing agents to prevent particle aggregation and provide stability. The XRD diffractogram (Figure 2d) of the RPF-AuNPs indicated that the predominant growth of the AuNPs occurred preferentially on the (111) plane, and the diffraction peaks (111), (200), (220), (311), and (222) of the XRD pattern confirmed the crystalline nature of the AuNPs (JCPDS 80-3697).

The particular process of the biosynthesis of AuNPs employing a biological material that already possesses a great number of biofunctional groups is still in the phase of uncertainty at this point. It is possible that the flavonoid compounds that were used in this study were the ones that occupied the hydroxyl and carbonyl groups in the production process for the AuNPs. Hydroxyl groups were responsible for the reduction of gold ions during the production of AuNPs, while carbonyl groups formed complexes by securely binding with metals. After the production of gold nanoparticles, flavonoids and bromine ions that were present in the reaction mixture enclosed the surface of the gold nanoparticles, while the alkyl adjusted its position such that it faced outward. There is a simultaneous manifestation of electrostatic and electrostatic stereo forces in the presence of IL. This is because anions and long alkyl chains are present in the environment. By capping the surfaces of the AuNPs with IL and other organic moieties, one can generate a colloidal solution that is stable and resistant to the effects of van der Waals forces. Therefore, a possible mechanism for the IL-mediated biosynthesis of RPF-AuNPs is proposed, as shown in Figure 3.

3.2. Peroxidase-Like Activity of RPF-AuNPs. As a chromogenic substrate, TMB was utilized to investigate the peroxidase-like activity exhibited by the artificially produced AuNPs. The experiment was carried out by establishing three separate reaction systems, each of which contained a different component. The addition of AuNPs to the colorless combination of TMB and H_2O_2 resulted in the observation of a notable blue color. Additionally, the distinctive absorption peak of oxTMB at 652 nm was seen at this time. This information is presented in Figure 4 (curve a). In contrast, there was no noticeable color or absorption at 652 nm detected in the samples (curves b and c) when AuNPs or H_2O_2 were absent. On the basis of the findings of the experiments, it was determined that the AuNPs demonstrated an intrinsic peroxidase-like activity.[32]

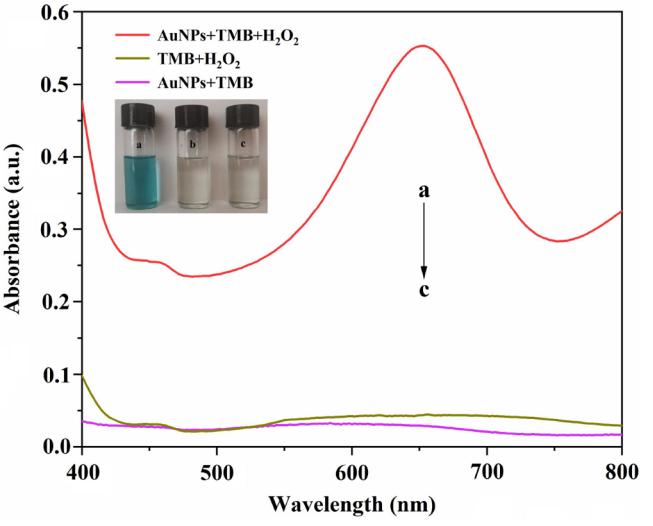

Figure 4. UV−vis absorption spectra of the peroxidase-like activity of RPF-AuNPs. AuNPs-TMB-H_2O_2 system (curve a), TMB-H_2O_2 system (curve b), and AuNPs-TMB system (curve c).

https://doi.org/10.1021/acsomega.2c05358
ACS Omega 2022, 7, 43045−43054

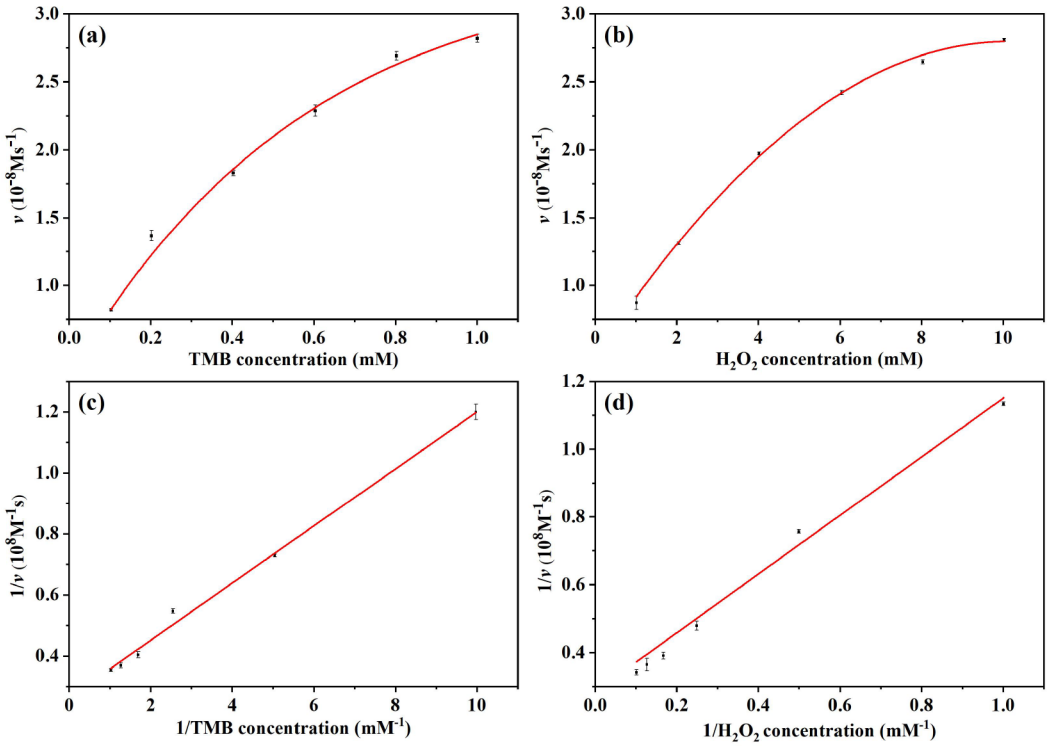

Figure 5. Steady-state kinetic assay of RPF-AuNPs (n = 3): (a) 10 mmol/L H_2O_2 with different concentrations of TMB. (b) 1 mmol/L TMB with different concentrations of H_2O_2. (c, d) Double-reciprocal plots of (a, b), respectively.

3.3. Kinetic Assay of Peroxidase-Like Activity. Kinetic experiments of RPF-AuNPs were carried out to understand further the catalytic mechanism, and TMB and H_2O_2 were chosen as substrates, respectively. Therefore, the standard Michaelis−Menten curves are shown in Figure 5. From the Lineweaver−Burk plots, the apparent steady-state kinetic parameters of RPF-AuNPs were calculated, and the Michaelis−Menten kinetics equation can be expressed as $1/v_0 = K_m/V_{max}(1/[S] + 1/K_m)$, where v_0 represents the initial velocity, V_{max} demonstrates the maximal initial velocity, K_m is the Michaelis−Menten constant, and $[S]$ corresponds to the substrate concentration. We calculated that the apparent K_m of RPF-AuNPs toward H_2O_2 and TMB was 2.61 and 0.35 mmol/L, respectively.

The lower the K_m value, the higher is the affinity between the enzyme and the substrate. Table 1 lists many kinetic parameters associated with horseradish peroxidase (HRP) and various nanozymes. It is important to note that RPF-AuNPs have a substantially higher affinity for both substrates in comparison to HRP and many other nanozymes that have been described. In addition, the value of V_{max} in our suggested system is not very high, and a low V_{max} value indicates a decrease in the product formation constant; a decrease in the product formation constant leads to lower apparent K_m values.[33] Therefore, a smaller value for V_{max} and a lower K_m are advantageous for increasing the catalytic activity of RPF-AuNPs.

Table 1. Comparison of Catalytic Kinetic Constants

catalyst	substance	K_m (mM)	V_{max} (M s^{-1})	reference
HRP	H_2O_2	3.70	8.71×10^{-8}	34
HRP	TMB	0.43	1.0×10^{-7}	34
Pd_{91}-GBLP	H_2O_2	10.75	4.93×10^{-8}	35
Pd_{91}-GBLP	TMB	2.43	2.26×10^{-7}	35
AuNCs-Pb^{2+}	H_2O_2	30.8	3.39×10^{-8}	36
AuNCs-Pb^{2+}	TMB	0.58	4.13×10^{-8}	36
Graphene-AuNPs	H_2O_2	26.4	1.54×10^{-7}	37
Graphene-AuNPs	TMB	0.38	1.83×10^{-7}	37
IL/RPF/AuNPs	H_2O_2	2.61	3.14×10^{-8}	this work
IL/RPF/AuNPs	TMB	0.35	3.72×10^{-8}	this work

3.4. Optimization of Electrochemical Detection Conditions. The effects of critical parameters such as pH, reaction temperature, reaction time, and electrochemical scan rate on the sensor response were studied and optimized using the absolute value of oxidation peak current $|I_{pa}|$ as the investigation index to obtain the excellent performance of the Cho electrochemical nonenzymatic sensor. Specifically, this was done in order to obtain excellent performance of the Cho electrochemical nonenzymatic sensor.

When it comes to determining the current response of the electrochemical sensor, the pH is one of the most important characteristics to consider. Within the pH range of 4.0 to 8.4, the influence of buffer pH on the electrochemical responses of RPF-AuNPs/GCE toward 5 mmol/L Cho was studied (Figure 6a). With the increase of pH from 4.0 to 7.2, the oxidation potential anion $|I_{pa}|$ of Cho increases. However, the maximum current drops when the pH is greater than 7.2. This characteristic of the current response shows that the acidic and basic systems inhibit the activity of the electrode, hence inhibiting the response.[38,39] Therefore, pH 7.2 was chosen as the optimum pH for Cho determination.

The electrocatalytic activity of the mimic enzyme is similarly temperature dependent. As depicted in Figure 6b, the reaction temperature was increased from 30 to 70 °C under pH-optimized conditions, and the current response was most robust around 30 °C, showing that the biosensor performed

https://doi.org/10.1021/acsomega.2c05358
ACS Omega 2022, 7, 43045−43054

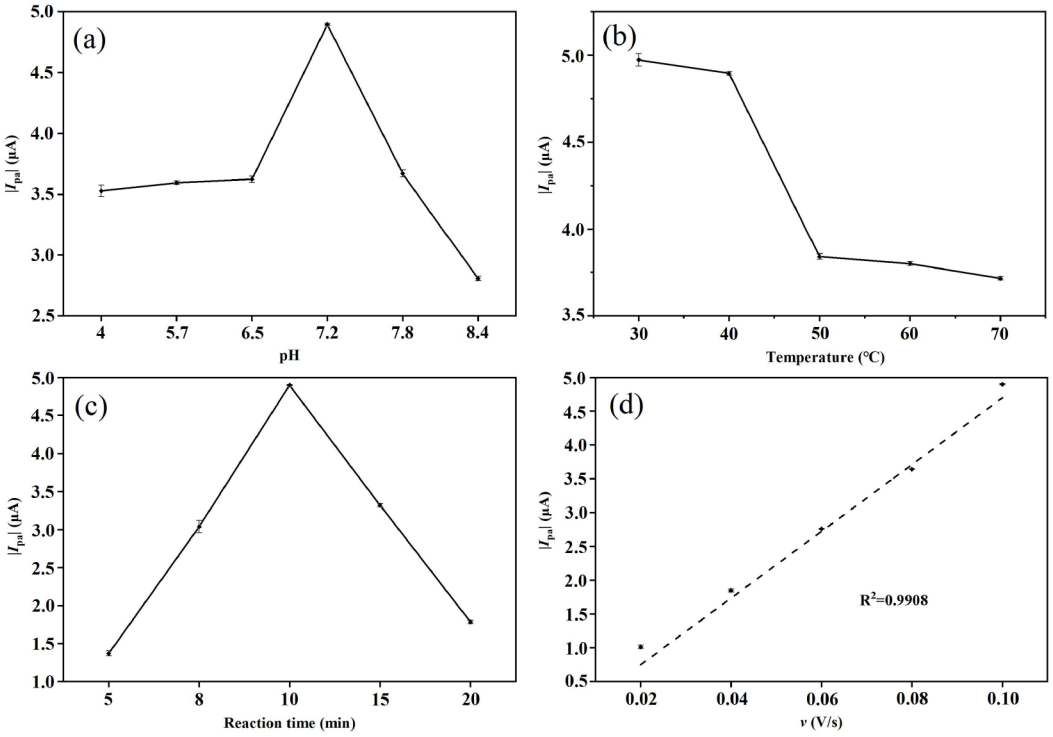

Figure 6. Effect of (a) pH value, (b) temperature, (c) reaction time, and (d) scan rate on the detection for Cho using an RPF-AuNP nonenzymatic electrochemical sensor (n = 3).

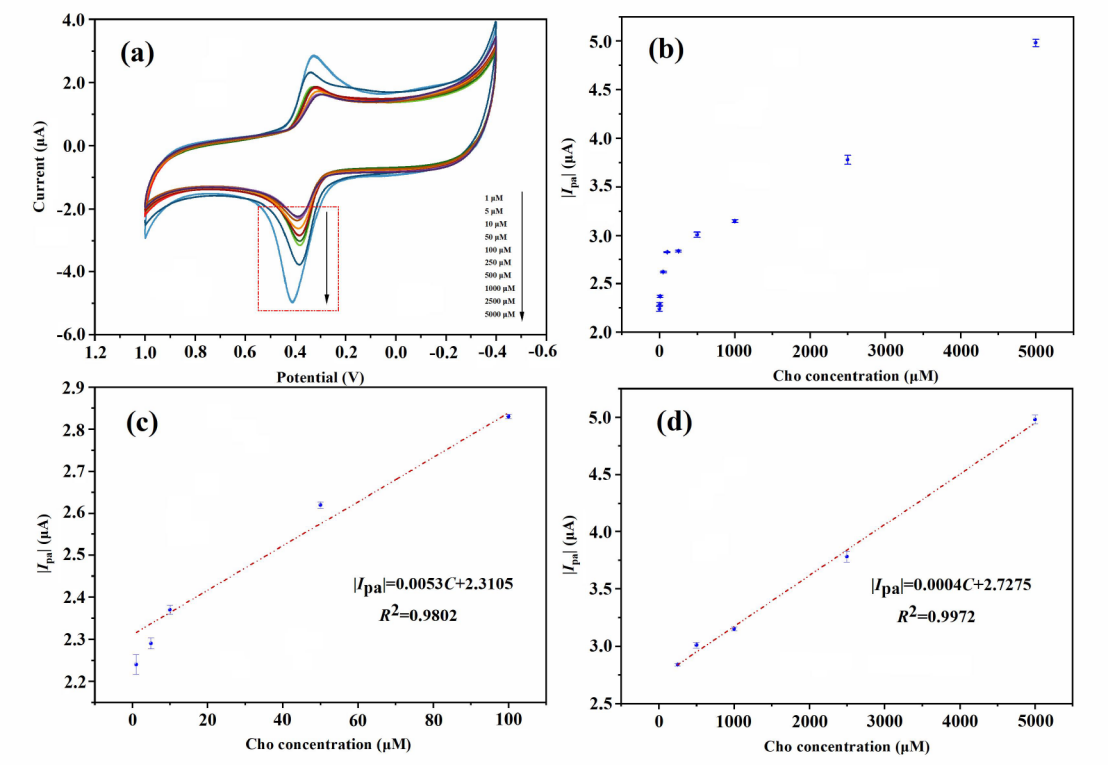

Figure 7. Response of RPF-AuNP nonenzymatic electrochemical sensor to different concentrations of Cho (n = 3): (a) CV curves of standard solutions with different concentrations of Cho. (b) The absolute value of oxidation peak current of different concentrations of Cho. (c, d) The working curve of electrochemical detection of Cho.

well at this temperature. In addition, a considerable drop in $|I_{pa}|$ was detected at high-temperature circumstances, which was attributed to the incomplete Cho oxidation process resulting from the decrease in oxygen content in the solution at high temperature. In addition, the mimic enzyme's stability reduced slightly as the temperature rose, which diminished its catalytic

https://doi.org/10.1021/acsomega.2c05358
ACS Omega 2022, 7, 43045−43054

Table 2. Comparison of Different Nanomaterial-Based Methods for the Determination of Cholesterol

nanomaterials	method	linear range (mmol/L)	LOD (μmol/L)	reference
CD-AuNCs	fluorescence	0.01−0.1	5.77	42
CeO_2-CDs	fluorescence	0.0016−1.65	0.49	43
GoldMag	colorimetry	0.018−1.4	7.9	44
Fe_3O_4@MIL-100(Fe)	colorimetry	0.05−0.4	1.3	45
MIL-101(Cr)	colorimetry	0.001−0.023	0.86	46
nanoporous gold	electrochemical	0.05−6.0	8.36	47
ChOx-SCCPPy-g-$C_3NH_4^+$/GCE	electrochemical	0.02−5.0	8.0	48
ChOx/AgNP/BDD/PAD	electrochemical	0.01−7	6.5	49
ChOx/CS/Ti(G)3DNS/G	electrochemical	0.05−8.0	6	50
CuO AuNPs/ssDNA-rGO	electrochemical	0.0075−0.2805	2.1	51
ZnO-nanowalls/ChOx	electrochemical	0.001−1	0.4	52
Ag/GO&CHER&CHOD/AuNPs/SPE	electrochemical	0.0258×10^{-3}−12.93	0.0026	53
IL/RPF/AuNPs	electrochemical	1×10^{-3}−0.1, 0.25−5	0.259	this work

activity. The optimal temperature for instant detection was determined to be 30 °C, as the detection environment was closer to room temperature and the influence of solvent volatilization could be disregarded.

The duration of the reaction time influences the viability of instantaneous detection. The effect of reaction time on the sensor's $|I_{pa}|$ was depicted in Figure 6c. The $|I_{pa}|$ grew dramatically as the reaction time increased from 5 to 10 min and then declined progressively as the reaction time increased further. Due to the insufficient advancement of the catalytic oxidation process, it is difficult to reach the maximal current response for reactions lasting less than 10 min. While the reaction time is too lengthy, the accumulated catalytic product H_2O_2 will hydrolyze to produce a weak current, interfering with the electrode's ability to recognize Cho and causing a drop in $|I_{pa}|$. Therefore, 10 min was chosen as the reaction time.

The rate at which the potential is scanned has an effect on the sensitivity of the electrochemical biosensor. An analysis was performed on the scan rate (ν) in the range of 0.02−0.1 V/s. According to the equations $|I_{pa}| = 49.340\nu - 0.237$ with a correlation coefficient of 0.9908, Figure 6d shows that the value of $|I_{pa}|$ for Cho changed linearly in response to changes in the scan rate. This observation supported the hypothesis that the GCE was home to a surface adsorption control process.[40] During the trials, it was discovered that, if the scan rate was increased to a value more than 0.1 V/s, the stability of the Cho nonenzymatic detecting system would be negatively impacted. As a result, taking into consideration the sensitivity and reproducibility of the Cho detection system, we decided that 0.1 V/s would be the best choice for the subsequent assay.

3.5. Detection of Cholesterol Based on the RPF-AuNP Nonenzymatic Electrochemical System. In order to assess the sensing efficacy of a manufactured RPF-AuNP nonenzymatic electrochemical sensor, different concentrations of standard Cho solution were quantified in accordance with the optimal experimental conditions mentioned above, and the current response was recorded using CV curves. A positive shift in the redox peaks, which may be attributed to the kinetics of the electrochemical processes, was discovered to be controlled by the adsorption of Cho, as shown in Figure 7a. This shift was shown to have been caused by the electrochemical reactions.[41] Figure 7b displays the $|I_{pa}|$ of various Cho concentrations. As expected, the current response increased gradually with increasing Cho concentrations, indicating the electrode based on RPF-AuNPs had excellent sensitivity to Cho. Notably, the $|I_{pa}|$ was proportional to the concentration of Cho in the two linear ranges from 1 to 100 μmol/L (Figure 7c) and 250 to 5000 μmol/L (Figure 7d). The linear regression equations were fitted as $|I_{pa}| = 0.0053C + 2.3105$ with the correlation coefficient of 0.9802 and $|I_{pa}| = 0.0004C + 2.7275$ with the correlation coefficient of 0.9972, respectively (where C is the Cho concentration in μmol/L). In addition, the limit of detection (LOD) was 0.259 μmol/L with a signal/noise ratio (S/N) of 3.

Inspiringly, the present analytical performances, including the linear range and LOD, are equivalent to or even superior to a great deal of the Cho assays that have been published in the past (Table 2). The strong electrical conductivity of the AuNPs was responsible for the good analytical performance that was achieved because it boosted the ability of electron transport on the electrode surface. In addition, gold nanoparticles with active flavonoid groups reacted with cholesterol in a redox reaction on the electrode surface, while Au^0 catalyzed the H_2O_2 reaction to produce oxidative activity radicals (·OH) to further catalyze the redox reaction on the electrode surface, which enhanced the current response of the oxidation peak and further improved the sensitivity of the sensor.

3.6. Anti-interference, Repeatability, Reproducibility, and Stability of the Sensor. An investigation was carried out to determine the impact of a number of different possible interferential species, including K^+, Na^+, Ca^{2+}, Mg^{2+}, glucose (Glu), vitamin C (VC), vitamin E (VE), L-cysteine (L-Cys), glycine (Gly), uric acid (UA), dopamine hydrochloride (DH), and glutathione (GSH) on the Cho determination. The working concentration of other interfering substances was ten times higher than that of Cho. These interferences exhibited negligible responses compared to Cho (Figure 8), which demonstrated that the RPF-AuNP-based nonenzymatic electrochemical system has superior anti-interference properties.

The repeatability analysis of the nonenzymatic electrochemical system was carried out by detecting 0.1, 1, and 2.5 mmol/L cholesterol for six successive measurements. In addition, the analytical applicability was examined by looking at the recoveries of Cho. As shown in Table 3, the RSD was determined to be 1.95%, 2.23%, and 2.38%, which were good indicators of a high degree of repeatability for the nonenzymatic electrochemical system. The recoveries ranged from 95.74% to 107.85% according to the findings. Therefore, the nonenzymatic electrochemical system has a high degree of accuracy and sensitivity.

https://doi.org/10.1021/acsomega.2c05358
ACS Omega 2022, 7, 43045−43054

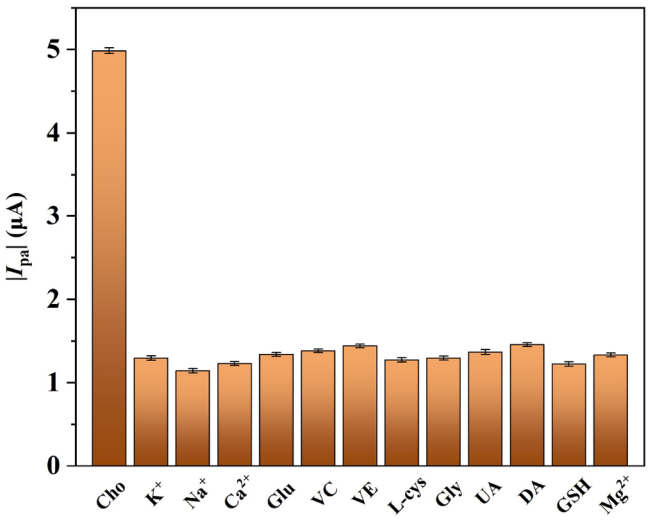

Figure 8. Anti-interference of the RPF-AuNP nonenzymatic electrochemical detection system of Cho (n = 3).

Table 3. Repeatability of RPF-AuNP Nonenzymatic Electrochemical Detection System of Cho

samples	added (mmol/L)	found (mmol/L)	recovery (%)	RSD (%)
standard solutions	0.1	0.0987	98.7	1.95
	1	1.054	105.4	2.23
	2.5	2.695	107.8	2.38

Reproducibility was also an important factor that determined the performance of the sensor toward cholesterol determination. To investigate the reproducibility of the as-prepared sensor, six nonenzymatic electrochemical systems were prepared by the same method for the detection of cholesterol, and the reproducibility of the system was further evaluated: the RSD of cholesterol was 1.82% (Figure 9a). This showed that the RPF-AuNP-based nonenzymatic electrochemical system has excellent reproducibility.

To evaluate the stability of the developed sensor, the nonenzymatic electrochemical system was stored for 10 days at room temperature and its stability was checked every day. The sensor maintained 93.71% stability of the initial current response after 10 days of preservation (Figure 9b). The results suggested that the sensor exhibited good stability for the cholesterol determination. It may be attributed to the dissolution and migration of the active catalytic site of the RPF-AuNPs over time, leading to particle aggregation.

3.7. Cholesterol Sensing in Food Samples. Egg yolk and pork liver were analyzed in order to finally see the practical applications of the suggested Cho sensor. The same technique was used to determine the $|I_{pa}|$ of 300 μL of the processed sample (Section 2.6), and the results obtained for all samples are reported in Table 4. Because the recoveries for the assay ranged from 98.2% to 105.4% and the results of this method were in general agreement with those of HPLC, it can be concluded that the analyses performed on the genuine food samples for Cho were acceptable and reliable.

Table 4. Determination and Recovery of Cholesterol in Food Samples

samples	content (mmol/g)	spiked (mmol/g)	found (mmol/g) HPLC	found (mmol/g) this work	recovery (%)
egg yolk	0.038	0.013	0.051	0.053	105.4
	0.048	0.013	0.060	0.059	98.2
pork liver	0.011	0.005	0.016	0.016	104.1
	0.012	0.005	0.017	0.017	98.9

4. CONCLUSIONS

A novel electrochemical nonenzymatic Cho sensor was created using newly synthesized AuNPs by following a procedure that was both straightforward and kind to the environment. The results of the UV−vis spectroscopy, TEM, FTIR, and XRD analyses all agreed that AuNPs had been synthesized. The suggested sensor demonstrates a number of advantageous characteristics, such as a limit of detection (LOD) of 0.259 μmol/L for Cho oxidation and a strong anti-interference capability. In addition, the Cho sensor also showed good performance when it was used for the analysis of food samples, indicating that the technology has the potential to be an appealing candidate for Cho sensing in real samples.

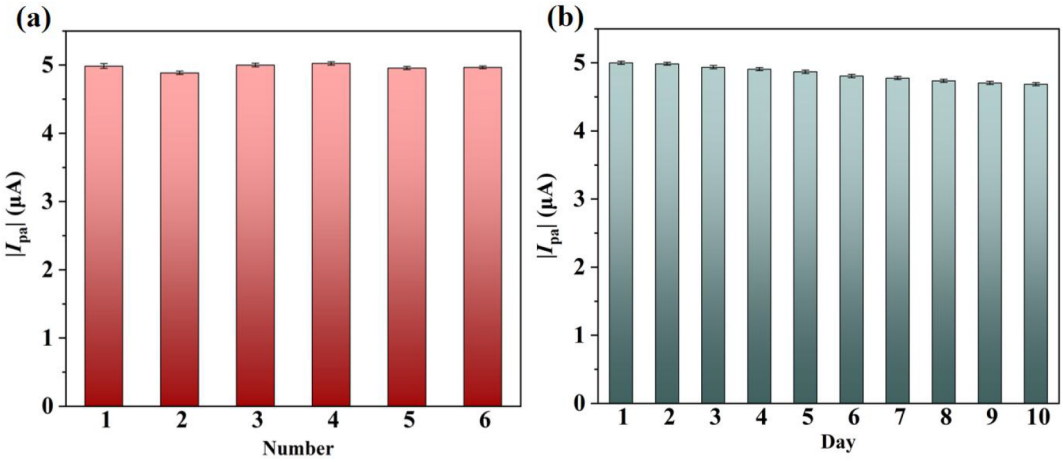

Figure 9. (a) Reproducibility of the RPF-AuNP nonenzymatic electrochemical detection system of Cho (n = 3) and (b) stability of the RPF-AuNP nonenzymatic electrochemical detection system of Cho (n = 3).

https://doi.org/10.1021/acsomega.2c05358
ACS Omega 2022, 7, 43045−43054

AUTHOR INFORMATION

Corresponding Authors

Huanan Guan − *College of Food Engineering, Harbin University of Commerce, Harbin 150028, China;* orcid.org/0000-0003-1182-8180; Phone: +86-451-84844281; Email: guanhuanan3@163.com

Ying Liu − *College of Food Engineering, Harbin University of Commerce, Harbin 150028, China*; Phone: +86-451-84844281; Email: 154057693@qq.com

Authors

Bolin Han − *College of Food Engineering, Harbin University of Commerce, Harbin 150028, China*

Yan Song − *College of Food Engineering, Harbin University of Commerce, Harbin 150028, China*

Complete contact information is available at: https://pubs.acs.org/10.1021/acsomega.2c05358

Notes

The authors declare no competing financial interest.

ACKNOWLEDGMENTS

This work was supported by the National Natural Science Foundation of China (No. 31201376), the Natural Science Foundation of Heilongjiang Province of China (No. LH2022C046), the "Young Innovative Talent" Support Program (No. 2019CX05), the Heilongjiang Postdoctoral Research Launch Project (No. LBH-Q19027), the Heilongjiang Leading Talent Support Program (No. 2020376), the Special Funds from the Central Finance to Support the Development of Local Universities (No. YSL036), and the Harbin Business University Graduate Research Innovation Project (No. HSD20210705).

REFERENCES

(1) Cai, F.; Li, S.; Huang, H.; Iqbal, J.; Wang, C.; Jiang, X. Green synthesis of gold nanoparticles for immune response regulation: Mechanisms, applications, and perspectives. *J. Biomed. Mater. Res., Part A* **2022**, *110* (2), 424−442.

(2) Gupta, R.; Singh, S.; Srivastava, P.; Singh, B. Role of tannic acid in desiging of electrically active and magnetic gold nanoparticles and enhanced photovoltaic performance of gold@titania photoanode in DSSC. *Mater. Chem. Phys.* **2022**, *278*, No. 125600.

(3) Hosny, M.; Fawzy, M.; El-Badry, Y. A.; Hussein, E. E.; Eltaweil, A. S. Plant-assisted synthesis of gold nanoparticles for photocatalytic, anticancer, and antioxidant applications. *J. Saudi Chem. Soc.* **2022**, *26* (2), No. 101419.

(4) Li, H.; Kou, B.; Yuan, Y.; Chai, Y.; Yuan, R. Porous Fe_3O_4@COF-Immobilized gold nanoparticles with excellent catalytic performance for sensitive electrochemical detection of ATP. *Biosens. Bioelectron.* **2022**, *197*, No. 113758.

(5) Kumawat, M.; Madhyastha, H.; Umapathi, A.; Singh, M.; Revaprasadu, N.; Daima, H. K. Surface engineered peroxidase-mimicking gold nanoparticles to subside cell inflammation. *Langmuir* **2022**, *38* (5), 1877−1887.

(6) Awad, M. A.; Eisa, N. E.; Virk, P.; Hendi, A. A.; Ortashi, K. M.; Mahgoub, A. S.; Elobeid, M. A.; Eissa, F. Z. Green synthesis of gold nanoparticles: Preparation, characterization, cytotoxicity, and antibacterial activities. *Mater. Lett.* **2019**, *256*, No. 126608.

(7) Chowdhury, N. K.; Choudhury, R.; Gogoi, B.; Chang, C.-M.; Pandey, R. P. Microbial synthesis of gold nanoparticles and their application. *Curr. Drug Targets* **2022**, *23* (7), 752−760.

(8) Khan, F.; Shariq, M.; Asif, M.; Siddiqui, M. A.; Malan, P.; Ahmad, F. Green Nanotechnology: Plant-Mediated Nanoparticle Synthesis and Application. *Nanomaterials* **2022**, *12* (4), 673.

(9) Tian, S.; Hu, Y.; Chen, X.; Liu, C.; Xue, Y.; Han, B. Green synthesis of silver nanoparticles using sodium alginate and tannic acid: Characterization and anti-S. aureus activity. *Int. J. Biol. Macromol.* **2022**, *195*, 515−522.

(10) Rafique, M.; Tahir, R.; Gillani, S. S. A.; Tahir, M. B.; Shakil, M.; Iqbal, T.; Abdellahi, M. O. Plant-mediated green synthesis of zinc oxide nanoparticles from Syzygium Cumini for seed germination and wastewater purification. *Int. J. Environ. Anal. Chem.* **2022**, *102* (1), 23−38.

(11) Irfan, M.; Moniruzzaman, M.; Ahmad, T.; Mandal, P. C.; Bhattacharjee, S.; Abdullah, B. Ionic liquid based extraction of flavonoids from Elaeis guineensis leaves and their applications for gold nanoparticles synthesis. *J. Mol. Liq.* **2017**, *241*, 270−278.

(12) Li, Y.; Zhang, C.; Ma, X.; Yang, L.; Ren, H. Identification of the potential mechanism of Radix pueraria in colon cancer based on network pharmacology. *Sci. Rep.* **2022**, *12* (1), 1−12.

(13) Zhang, Z.; Lam, T. N.; Zuo, Z. Radix Puerariae: an overview of its chemistry, pharmacology, pharmacokinetics, and clinical use. *J. Clin Pharmacol* **2013**, *53* (8), 787−811.

(14) Liu, Y.-S.; Yuan, M.-H.; Zhang, C.-Y.; Liu, H.-M.; Liu, J.-R.; Wei, A.-L.; Ye, Q.; Zeng, B.; Li, M.-F.; Guo, Y.-P. Puerariae Lobatae radix flavonoids and puerarin alleviate alcoholic liver injury in zebrafish by regulating alcohol and lipid metabolism. *Biomed. Pharmacother.* **2021**, *134*, No. 111121.

(15) Rajabi, M. S.; Moniruzzaman, M.; Mahmood, H.; Sivapragasam, M.; Bustam, M. A. Extraction of β-carotene from organic phase using ammonium based ionic liquids aqueous solution. *J. Mol. Liq.* **2017**, *227*, 15−20.

(16) Pan, J.; Han, W.; Jiang, Y.; Wu, J.; Zhou, X. Association of dietary cholesterol and dyslipidemia in Chinese health examinees. *J. Health. Popul. Nutr.* **2022**, *41* (1), 1−7.

(17) López-Fernández, O.; Domínguez, R.; Santos, E. M.; Pateiro, M.; Munekata, P. E.; Campagnol, P. C.; Lorenzo, J. M. Comparison Between HPLC-PAD and GC-MS Methods for the Quantification of Cholesterol in Meat. *Food. Anal. Method.* **2022**, *15* (4), 1118−1131.

(18) Guan, H.; Song, Y.; Han, B.; Gong, D.; Zhang, N. Colorimetric detection of cholesterol based on peroxidase mimetic activity of GoldMag nanocomposites. *Spectrochim. Acta, Part A* **2020**, *241*, No. 118675.

(19) Ding, J.; Zhang, W.; Xue, F.; Sun, Y.; Yan, Q.; Chen, Y.; Shan, G. Highly dispersive AuNCs/ChOx@ ZIF-8/PEI nanocomplexes for fluorescent detection of cholesterol in human serum. *Microchim. Acta* **2022**, *189* (5), 1−10.

(20) Khaliq, N.; Rasheed, M. A.; Khan, M.; Maqbool, M.; Ahmad, M.; Karim, S.; Nisar, A.; Schmuki, P.; Cho, S. O.; Ali, G. Voltage-switchable biosensor with gold nanoparticles on TiO_2 nanotubes decorated with CdS quantum dots for the detection of cholesterol and H_2O_2. *ACS Appl. Mater. Interfaces* **2021**, *13* (3), 3653−3668.

(21) Amiri, M.; Arshi, S. An Overview on Electrochemical Determination of Cholesterol. *Electroanalysis* **2020**, *32* (7), 1391−1407.

(22) Derina, K.; Korotkova, E.; Barek, J. Non-enzymatic electrochemical approaches to cholesterol determination. *J. Pharm. Biomed Anal* **2020**, *191*, No. 113538.

(23) Yadav, H. M.; Park, J.-D.; Kang, H.-C.; Lee, J.-J. Recent Development in Nanomaterial-Based Electrochemical Sensors for Cholesterol Detection. *Chemosensors* **2021**, *9* (5), 98−116.

(24) Li, G.; Qi, X.; Wu, J.; Xu, L.; Wan, X.; Liu, Y.; Chen, Y.; Li, Q. Ultrasensitive, label-free voltammetric determination of norfloxacin based on molecularly imprinted polymers and Au nanoparticle-functionalized black phosphorus nanosheet nanocomposite. *J. Hazard. Mater.* **2022**, *436*, No. 129107.

(25) Li, G.; Qi, X.; Zhang, G.; Wang, S.; Li, K.; Wu, J.; Wan, X.; Liu, Y.; Li, Q. Low-cost voltammetric sensors for robust determination of toxic Cd (II) and Pb (II) in environment and food based on shuttle-like α-Fe_2O_3 nanoparticles decorated β-Bi_2O_3 microspheres. *Microchem. J.* **2022**, *179*, No. 107515.

(26) Li, G.; Wu, J.; Qi, X.; Wan, X.; Liu, Y.; Chen, Y.; Xu, L. Molecularly imprinted polypyrrole film-coated poly(3,4-ethylenediox-

ythiophene):polystyrene sulfonate-functionalized black phosphorene for the selective and robust detection of norfloxacin. *Mater. Today Chem.* **2022**, *26*, No. 101043.
(27) Li, Q.; Wu, J.-T.; Liu, Y.; Qi, X.-M.; Jin, H.-G.; Yang, C.; Liu, J.; Li, G.-L.; He, Q.-G. Recent advances in black phosphorus-based electrochemical sensors: A review. *Anal. Chim. Acta* **2021**, *1170*, No. 338480.
(28) Prasad, K.; Mishra, M. Mechanism of Hypercholesterolemia-Induced Atherosclerosis. *Rev. Cardiovasc. Med.* **2022**, *23* (6), 212−222.
(29) Wang, Y.; Wang, Y.; Zhang, S.; Zhao, N.; Fu, Y.; Ying-Xin, J.; Zhang, N. Cu^{2+} induced Regulation and construction of FAD-Mb/Cu-Mb@AuNPs Bi-functional mimetic enzyme and application in glucose visualization detection. *Microchem. J.* **2022**, *175*, No. 107207.
(30) Yu, J.; Xu, D.; Guan, H. N.; Wang, C.; Huang, L. K. Facile one-step green synthesis of gold nanoparticles using Citrus maxima aqueous extracts and its catalytic activity. *Mater. Lett.* **2016**, *166*, 110−112.
(31) Chellapandian, C.; Ramkumar, B.; Puja, P.; Shanmuganathan, R.; Pugazhendhi, A.; Kumar, P. Gold nanoparticles using red seaweed Gracilaria verrucosa: green synthesis, characterization and biocompatibility studies. *Process Biochem.* **2019**, *80*, 58−63.
(32) Zhang, H.; Wu, H.; Qin, X.; Shen, Y.; Wei, X.; Liu, G. Metalloporphyrin and gold nanoparticles modified hollow zeolite imidazole Framework-8 with excellent peroxidase like activity for quick colorimetric determination of choline in infant formula milk powder. *Food. Chem.* **2022**, *384*, No. 132552.
(33) Liu, H.; Ding, Y.; Yang, B.; Liu, Z.; Liu, Q.; Zhang, X. Colorimetric and ultrasensitive detection of H_2O_2 based on Au/Co_3O_4-CeO_x nanocomposites with enhanced peroxidase-like performance. *Sens. Actuators, B* **2018**, *271*, 336−345.
(34) Gao, L.; Zhuang, J.; Nie, L.; Zhang, J.; Zhang, Y.; Gu, N.; Wang, T.; Feng, J.; Yang, D.; Perrett, S. Intrinsic peroxidase-like activity of ferromagnetic nanoparticles. *Nat. Nanotechnol.* **2007**, *2* (9), 577−583.
(35) Cui, Y.; Lai, X.; Liu, K.; Liang, B.; Ma, G.; Wang, L. Ginkgo biloba leaf polysaccharide stabilized palladium nanoparticles with enhanced peroxidase-like property for the colorimetric detection of glucose. *RSC Adv.* **2020**, *10* (12), 7012−7018.
(36) Liao, H.; Liu, G.; Liu, Y.; Li, R.; Fu, W.; Hu, L. Aggregation-induced accelerating peroxidase-like activity of gold nanoclusters and their applications for colorimetric Pb^{2+} detection. *Chem. Commun.* **2017**, *53* (73), 10160−10163.
(37) Chen, X.; Tian, X.; Su, B.; Huang, Z.; Chen, X.; Oyama, M. Au nanoparticles on citrate-functionalized graphene nanosheets with a high peroxidase-like performance. *Dalton Trans.* **2014**, *43* (20), 7449−7454.
(38) Anh, T. T. N.; Lan, H.; Tam, L. T.; Pham, V.-H.; Tam, P. D. Highly sensitive nonenzymatic cholesterol sensor based on zinc oxide nanorods. *J. Electron. Mater.* **2018**, *47* (11), 6701−6708.
(39) Dervisevic, M.; Çevik, E.; Şenel, M.; Nergiz, C.; Abasiyanik, M. F. Amperometric cholesterol biosensor based on reconstituted cholesterol oxidase on boronic acid functional conducting polymers. *J. Electroanal. Chem.* **2016**, *776*, 18−24.
(40) Vatandost, E.; Ghorbani-HasanSaraei, A.; Chekin, F.; Raeisi, S. N.; Shahidi, S.-A. Green tea extract assisted green synthesis of reduced graphene oxide: Application for highly sensitive electrochemical detection of sunset yellow in food products. *Food Chem.: X* **2020**, *6*, No. 100085.
(41) Khaliq, N.; Rasheed, M. A.; Cha, G.; Khan, M.; Karim, S.; Schmuki, P.; Ali, G. Development of non-enzymatic cholesterol biosensor based on TiO_2 nanotubes decorated with Cu_2O nanoparticles. *Sens. Actuators, B* **2020**, *302*, No. 127200.
(42) Xiao, W.; Yang, Z.; Liu, J.; Chen, Z.; Li, H. Sensitive cholesterol determination by β-cyclodextrin recognition based on fluorescence enhancement of gold nanoclusters. *Microchem. J.* **2022**, *175*, No. 107125.
(43) Yang, Z.; Liu, Y.; Lu, C.; Yue, G.; Wang, Y.; Rao, H.; Zhang, W.; Lu, Z.; Wang, X. One-pot synthesis of CeO_2-carbon dots with enhanced peroxidase-like activity and carbon dots for ratiometric fluorescence detection of H_2O_2 and cholesterol. *J. Alloys Compd.* **2021**, *862*, No. 158323.
(44) Guan, H.; Song, Y.; Han, B.; Gong, D.; Zhang, N. Colorimetric detection of cholesterol based on peroxidase mimetic activity of GoldMag nanocomposites. *Spectrochim. Acta, Part A* **2020**, *241*, No. 118675.
(45) Xu, J.; Peng, J.; Wang, X.; Hou, X. Enhanced Peroxidase-like Activity of Fe_3O_4@MIL-100(Fe) Aroused by ATP for One-Step Colorimetric Sensing toward Cholesterol. *ACS Sustainable Chem. Eng.* **2022**, *10* (29), 9315−9324.
(46) Liu, L.; Wang, J.; Wang, J.; Wu, J.; Wu, S.; Xie, L. Colorimetric Detection of Cholesterol Based on the Peroxidase-Like Activity of Metal-Organic Framework MIL-101(Cr). *ChemistrySelect* **2021**, *6* (28), 7143−7149.
(47) Wang, S.; Chen, S.; Shang, K.; Gao, X.; Wang, X. Sensitive electrochemical detection of cholesterol using a portable paper sensor based on the synergistic effect of cholesterol oxidase and nanoporous gold. *Int. J. Biol. Macromol.* **2021**, *189*, 356−362.
(48) Shrestha, B. K.; Ahmad, R.; Shrestha, S.; Park, C. H.; Kim, C. S. In situ synthesis of cylindrical spongy polypyrrole doped protonated graphitic carbon nitride for cholesterol sensing application. *Biosens. Bioelectron.* **2017**, *94*, 686−693.
(49) Nantaphol, S.; Chailapakul, O.; Siangproh, W. A novel paper-based device coupled with a silver nanoparticle-modified boron-doped diamond electrode for cholesterol detection. *Anal. Chim. Acta* **2015**, *891*, 136−143.
(50) Komathi, S.; Muthuchamy, N.; Lee, K.; Gopalan, A. Fabrication of a novel dual mode cholesterol biosensor using titanium dioxide nanowire bridged 3D graphene nanostacks. *Biosens. Bioelectron.* **2016**, *84*, 64−71.
(51) Wu, S.; Sui, C.; Wang, C.; Wang, Y.; He, D.; Sun, Y.; Zhang, Y.; Meng, Q.; Ma, T.; Song, X.-M. Gold nanoparticles/single-stranded DNA-reduced graphene oxide nanocomposites based electrochemical biosensor for highly sensitive detection of cholesterol. *Front. Chem. Sci. Eng.* **2021**, *15* (6), 1572−1582.
(52) Psychoyios, V. N.; Nikoleli, G. P.; Tzamtzis, N.; Nikolelis, D. P.; Psaroudakis, N.; Danielsson, B.; Israr, M. Q.; Willander, M. Potentiometric cholesterol biosensor based on ZnO nanowalls and stabilized polymerized lipid film. *Electroanalysis* **2013**, *25* (2), 367−372.
(53) Huang, Y.; Tan, J.; Cui, L.; Zhou, Z.; Zhou, S.; Zhang, Z.; Zheng, R.; Xue, Y.; Zhang, M.; Li, S. Graphene and AuNPs co-mediated enzymatic silver deposition for the ultrasensitive electrochemical detection of cholesterol. *Biosens. Bioelectron.* **2018**, *102*, 560−567.

https://doi.org/10.1021/acsomega.2c05358
ACS Omega 2022, 7, 43045−43054